doi: 10.1111/j.1365-3121.2009.00916.x

Concurrent tectonic and climatic changes recorded in upper Tortonian sediments from the Eastern Mediterranean

Cornelia M. Köhler,[1] Wout Krijgsman,[2] Douwe J. J. van Hinsbergen,[2] David Heslop[3] and Guillaume Dupont-Nivet[2]

[1]*Department of Geology and Petroleum Geology, Meston Building, King's College, University of Aberdeen, Aberdeen AB24 3UE, UK;* [2]*Paleomagnetic Laboratory 'Fort Hoofddijk', University of Utrecht, Budapestlaan 17, 3584 CD Utrecht, The Netherlands;* [3]*University of Bremen, FB Geowissenschaften, Postfach 330440, Bremen, Germany*

ABSTRACT

The upper Tortonian Metochia marls on the island of Gavdos provide an ideal geological archive to trace variations in Aegean sediment supply as well as changes in the North African monsoon system. A fuzzy-cluster analysis on the multiproxy geochemical and rock magnetic dataset of the astronomically tuned sedimentary succession shows a dramatic shift in the dominance of 'Aegean tectonic' clusters to 'North African climate' clusters. The tectonic signature, traced by the starvation of the Cretan sediment, now enables to date the late Tortonian basin foundering on Crete, related to the tectonic break-up of the Aegean landmass, at *c.* 8.2 Ma. The synchronous decrease in the North African climate proxies is interpreted to indicate a change in the depositional conditions of the sink rather than a climatic change in the African source. This illustrates that interpretations of climate proxies require a multiproxy approach which also assesses possible contributions of regional tectonism.

Terra Nova, 22, 52–63, 2010

Introduction

The semi-enclosed land-locked configuration of the Mediterranean region at the European-African collision zone makes it suitable to register sedimentary provenance changes resulting from both plate tectonic processes and changes in palaeoclimate (e.g. Krijgsman, 2002). The Miocene geodynamic evolution of the Mediterranean region was controlled largely by the subduction of the African plate under the European margin. These plate tectonic processes were ongoing throughout the entire Miocene, but were also marked by a strong, Mediterranean-wide, increase of tectonic activity in the late Tortonian (Carminati *et al.*, 1998; Wortel and Spakman, 2000; Hüsing *et al.*, 2009). Late Tortonian climatic reconstructions reveal substantial changes, especially on the North African continent which is thought to have been much more humid than today (e.g. Griffin, 2002; Gladstone *et al.*, 2007). A proxy to trace African climate is aeolian dust input off the coasts of Africa, which decreases with increasing humidity as shown by Pliocene case studies (Ruddiman *et al.*, 1989; deMenocal *et al.*, 1991).

Studies of Mediterranean sedimentary archives have demonstrated that geochemical proxies can be indicative of different sediment origins and that they can be linked to changes in the environmental conditions of Mediterranean and African source areas (e.g. Bergametti *et al.*, 1989; Wehausen and Brumsack, 1998; Lourens *et al.*, 2001; Larrasoaña *et al.*, 2003; Köhler *et al.*, 2008). Recently, the astronomically dated marls of the Metochia section on the island of Gavdos (Fig. 1) were studied to track provenance changes in the eastern Mediterranean during the late Miocene (Köhler *et al.*, 2008). The palaeogeographical location of the section within the fluvio-lacustrine drainage system of the southern Aegean landmass (e.g. Fortuin, 1978) and its relative proximity to the North African margin make it ideal to trace variations in Aegean sediment supply as well as changes in the North African monsoon. The multiparameter dataset from Metochia revealed concurrent changes in Aegean and African sediment supply in the late Tortonian, raising the question whether a causal relationship exists. We attempted to reassess the timing and nature of climatically and tectonically induced changes in late Tortonian sediment provenance and their temporal evolution in the eastern Mediterranean region.

Correspondence: Cornelia M. Köhler, Department of Geology and Petroleum Geology, University of Aberdeen, Meston Building, King's College, Aberdeen AB24 3UE, UK. Tel.: +44 1224 273437; fax: +44 1224 277785; e-mail: ckoehler@uni-bremen.de

Concurrent tectonic and climatic changes in the Metochia marls

The Metochia section on the island of Gavdos, located south of Crete (Fig. 1), provides an ideal archive spanning the period between 9.7 and 6.6 Ma (Hilgen *et al.*, 1995; Krijgsman *et al.*, 1995). The age model of the Metochia section (Hilgen *et al.*, 1995; Krijgsman *et al.*, 1995) was updated with revised orbital ages [Fig. 2, Laskar *et al.* (2004)]. The sedimentation rate, presumed to be dominated by Aegean terrigenous supply being drained by fluvial systems into the Gavdos basin (Fortuin, 1978; van Hinsbergen and Meulenkamp, 2006), shows a steady decline and remains at low values from *c.* 8.15 Ma onwards (Fig. 2).

The marls of the Metochia section contain a mixture of sediments from the Aegean and North African regions (Köhler *et al.*, 2008). Aegean provenance is traced by Nickel (Ni) and Chrome (Cr), as their presence can be linked to sediments derived from ultramafic rocks, well-known from Crete (Koepke *et al.*, 2002), having high Ni and Cr concentrations (Wedepohl, 1969; Wehausen and Brumsack, 2000). The Ni- and Cr-MARs (mass accumulation rate) show variable but declining values upsection with a drop to intermediate values between 8.4 and 8.2 Ma and to minimal values at 8.15 Ma. Provenance

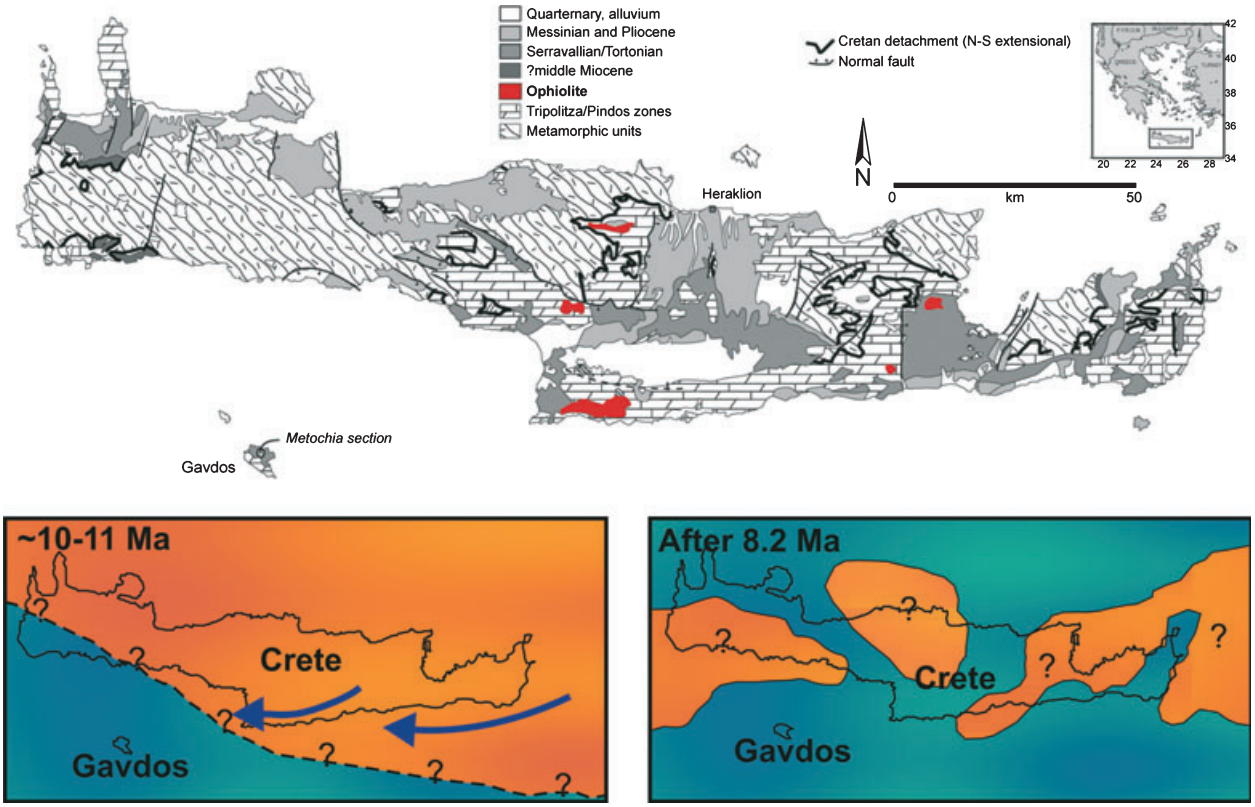

Fig. 1 Top: geological map of Crete and Gavdos (Meulenkamp, *et al.*, 1988, van Hinsbergen and Meulenkamp, 2006). The Ni-rich source areas (ophiolites) are marked in red; they are located within the drainage area of the fluvio-lacustrine system. Bottom: the two settings described in the text (landmass in orange and sea in blue). Left: Crete and the Aegean region forming a landmass and being drained to the West. Right: the Aegean landmass being fragmented (modified from: Meulenkamp and Hilgen, 1986, Meulenkamp, *et al.*, 1988, van Hinsbergen and Meulenkamp, 2006).

from North Africa is traced by the aeolian dust proxies hard isothermal remanent magnetisation (HIRM) and anhysteretic remanent magnetisation (ARM) (e.g. Larrasoaña *et al.*, 2003). These magnetic proxies have intermediate to maximum peaks and fluctuations prior to 8.2 Ma (Fig. 2), the HIRM being more variable between 9.3 and 8.65 Ma. Between 8.65 and 8.15 Ma, both parameters have maximal values suggesting increased North African dust input (Fig. 2), followed by a marked drop in North African dust input interestingly also at 8.15 Ma (Fig. 2).

Fuzzy *c*-means clustering (FCM) is a multivariate statistical approach with which to partition data based on similarities and dissimilarities within a multivariate space (Bedzek *et al.*, 1984). Cluster centres represent locations in the data space to which each sample can be compared and assigned a membership value based on a distance metric (membership values range between 0 indicating 'no similarity' and 1 corresponding to 'identical'). The FCM solution provides an optimal balance between maximising the separation of the cluster centres and minimising the distance between the samples and their nearest cluster centre. NLM is a projection technique with which a multidimensional dataset can be mapped into a lower dimensional space whilst preserving its inherent structure (Sammon, 1969). This is archived by determining the low dimensional sample configuration which best preserves the distances between the samples in the original measurement space. When both the FCM and NLM show similar groupings, then the cluster solution is assumed to be robust (Köhler *et al.*, 2008). The following input parameters were chosen for the FCM/NLM analysis: Ti/Al for aeolian vs. fluvial transport (e.g. Larrasoaña *et al.*, 2003), HIRM for North African dust input, Ni/Al for Aegean sediment supply, Al-MAR for total terrigenous sediment supply, $CaCO_3$ for marine productivity and Mn/Al for diagenetic processes (e.g. van Santvoort *et al.*, 1997). Through the combination of these proxies, the data were integrated into a four-cluster model (Köhler *et al.*, 2008).

Two contrasting 'pairs of clusters' were defined based on the cluster centre locations in the multivariate space: high vs. low Aegean input clusters and high vs. low North African dust input clusters (Fig. 3a,b). The Aegean input clusters have high Ni/Al and Al-MAR values and represent the highest terrigenous input. The African clusters are represented by high HIRM and Ti/Al values. Sample membership to these clusters (Fig. 3a) show that the high terrigenous cluster centres ('high Aegean' and 'high North African dust') dominated from 9.4 to 8.2 Ma and that 'low Aegean' and 'low North African dust' cluster centres became important

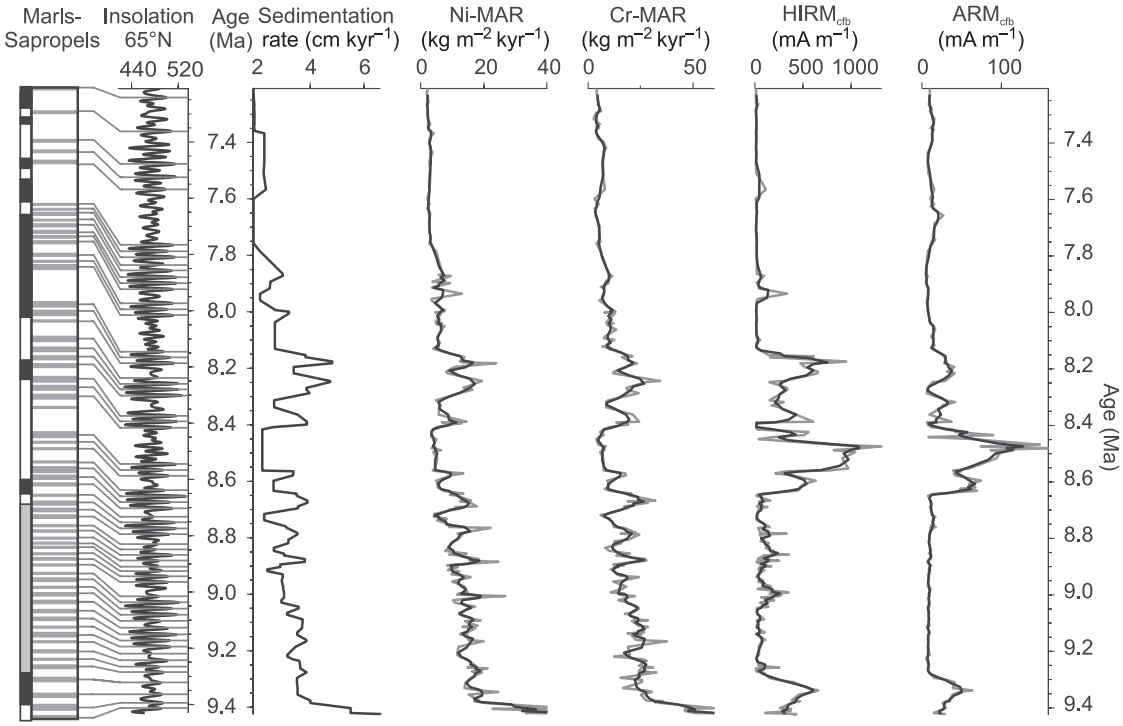

Fig. 2 Lithology and magnetostratigraphy (modified from Krijgsman, *et al.* (1995)) and age profiles of proxies of the Metochia section described in the text. The lithology: white intervals represent homogeneous marls, the dark grey sapropels. The magnetostratigraphy: black = normal and white = reversed polarity; grey = unreliable directions. The Metochia section was correlated to the GPTS of CK95 (Cande and Kent, 1995) by Krijgsman, *et al.* (1995). The Ni- and Ch-MARs trace the Aegean landmass sediment supply. The magnetic parameters trace the North African dust component; the HIRM was calculated using a saturation field of 2500 mT and a backfield of 300 mT (Köhler *et al.*, 2008), the ARM was imparted under a DC bias field of 50 μT and a peak alternating field of 100 mT. The light grey lines indicate the data, the thick, black lines represent a three point running mean plot to highlight the important changes.

after 8.2 Ma. Thus, the drop in Aegean sediment supply coincides with a drop in North African dust at *c.* 8.2 Ma (Fig. 3a). Vertical shifts on the NLM plot appear to represent movement between high terrigenous and *in situ* marine sediment sources (Fig. 3b), with little influence of Aegean or North African provenance. NLM *y*-axis values plotted as a function of age reveal a change from high Aegean to low Aegean input between *c.* 8.2 and 7.9 Ma (Fig. 3c).

Late Tortonian tectonic changes in the Aegean source

Our analyses indicate that a significant change in the Aegean area occurred at *c.* 8.2 Ma. The Cretan upper Tortonian documents a transition of extension directions and deformation style, associated with curvature of the Aegean arc (e.g. van Hinsbergen and Meulenkamp, 2006) during south (west)ward roll-back of the African slab (Le Pichon and Angelier, 1981; Jolivet, 2001; van Hinsbergen *et al.*, 2005). Early to middle Miocene N–S extension on Crete was accommodated along low-angle extensional detachments, exhuming high pressure–low temperature metamorphic rocks (Fassoulas *et al.*, 1994; Jolivet *et al.*, 1996; Thomson *et al.*, 1998; Rahl *et al.*, 2005). These were dissected by upper Tortonian high-angle normal faults during E–W extension, foundering deep-marine basins (Meulenkamp *et al.*, 1988; Fassoulas *et al.*, 1994), estimated by van Hinsbergen and Meulenkamp (2006) to occur between 9 and 7 Ma. Upper Tortonian syn-tectonic sedimentary sequences that may document this phase mainly consist of coarse clastics and are unsuitable to provide more accurate ages for this phase.

The sudden starvation of the Aegean sediment source on Gavdos suggests that the drainage systems on Crete, providing erosion material from the southern Aegean landmass, were disconnected from the Gavdos sink at *c.* 8.2 Ma, probably dating the Cretan late Tortonian break-up event. This age is in line with vertical motion resconstructions of the Kastelli section (on south-central Crete (van Hinsbergen and Meulenkamp, 2006): Palaeobathymetric reconstructions by means of planktonic/benthic foraminifera ratios show a deepening from ~400 to 900 m between *c.* 7.9 and 7.5 Ma, after which the section was deep-marine until at least 7.1 Ma. Assuming a constant sedimentation rate and using the age-stratigraphic constraints of Langereis (1984) and Krijgsman *et al.* (1994), the main transgression at Kastelli' would have occurred between *c.* 8.4 and 8.1 Ma (Fig. 4).

Starvation of Aegean sediment supply on Gavdos was therefore probably related to tectonic changes causing an episode of basin foundering on Crete. Our multiproxy analyses on the Metochia marls, combined with inter-

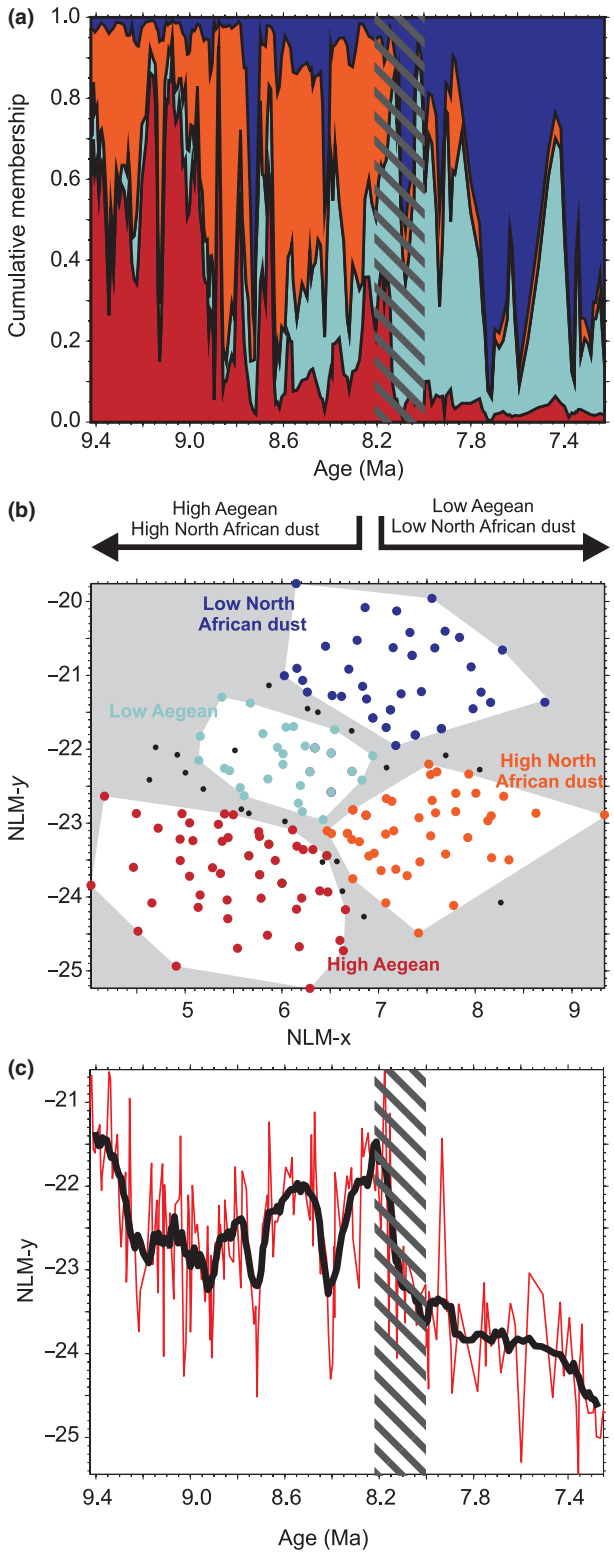

Fig. 3 The results from the FCM and NLM analysis (Köhler *et al.*, 2008, see Appendix A for data). (a) The cumulative membership plot obtained from FCM shows how the memberships of the individual samples vary over time. The colours are indicative of climate change in North Africa: blue colours indicate humid North Africa with low dust input, whereas the red colour variations show arid North Africa with high dust input. (b) The NLM provides a low-dimensional representation of the proxy data set, individual samples are marked with points which are colour-coded according to the fuzzy cluster-centre to which they are assigned (transitional samples which have no clear assignment to any cluster centre are shown as smaller black circles) (Köhler *et al.*, 2008). (c) The NLM *y*-axis values of the samples plotted as a function of age reveal a change from high Aegean to low Aegean input (the black line is a 3-point running mean). The hatched bar indicates the time interval when the high Aegean cluster becomes replaced by the low Aegean cluster, describing a change in terrigenous input from the Aegean region.

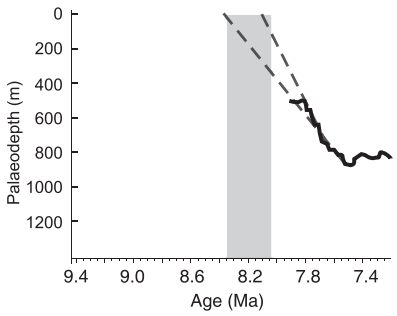

Fig. 4 Paleobathymetry curve of the Kastelli section modified from (van Hinsbergen and Meulenkamp, 2006). Extrapolating the subsidence curve (assuming more or less constant subsidence) gives an age onset of submergence clearly coinciding with the transitional period identified in the FCM. This period covers the time interval when the high Aegean cluster becomes replaced by the low Aegean cluster, describing a change in terrigenous input from the Aegean region.

polated subsidence rates of the Cretan basins, now show that the Cretan-wide onset of E–W extensional basins can be accurately dated at 8.2 Ma.

Late Tortonian climatic changes in the North African source

Analyses of the Metochia marls suggest a major change in North African sediment supply at *c.* 8.2 Ma, previously interpreted as a shift to a more humid North Africa (Köhler *et al.*, 2008) possibly associated with intensification of the North African monsoon system (Rohling *et al.*, 2002). A late Miocene change towards more humid conditions

is also documented off the West and East African coasts by reduced dust input (Ruddiman *et al.*, 1989; deMenocal *et al.*, 1991). Conversely, the Lake Chad area was covered by upper Tortonian lakes (Lihoreau *et al.*, 2006) and river systems drained towards the Mediterranean Sea (Griffin, 2002; Gladstone *et al.*, 2007).

However, to create such humid conditions in North Africa, the northern limit of the intertropical convergence zone which largely influences the African monsoon system, would need to shift as far as ~22°N, passing the central Saharan watershed (Rohling *et al.*, 2002; Larrasoaña *et al.*, 2003). In addition, it has been argued that the North African monsoon system was linked to the Asian monsoon system (Griffin, 2002), which showed an enhancement during the late Miocene (Kroon *et al.*, 1991, An, *et al.*, 2001). Fluteau *et al.* (1999) showed that an intensification of the Asian monsoon system would also enhance the Easterly Tropical Jet, thus decreasing moisture availability over North Africa. Alternatively, Sepulchre *et al.* (2006) argued that the uplift of the Ethiopian Plateau barrier led to a drastic reorganisation of the atmospheric circulation associated with strong North African aridification after 8 Ma. Consequently, we find no conclusive evidence from climatic and palaeoenvironmental studies supporting a decreased dust flux because of intensification of the monsoon system in North Africa at 8.2 Ma.

Coeval changes resulting from Mediterranean sink adjustment

In addition to the absence of evidence for climate change in the North African source area at 8.2 Ma, a compelling fact is that our proxy record indicates precisely coeval Mediterranean tectonism. We find it unlikely that the alleged African monsoon intensification is precisely simultaneous with, but completely unrelated to Aegean tectonics, or that Aegean tectonics had such a strong climatic effect on North African climate. In contrast, a mechanism that can explain these coeval changes is a late Tortonian reorganisation of Mediterranean depositional environments, including the sink region at Gavdos.

The late Tortonian is characterised by Mediterranean-wide palaeogeographical and palaeoceanographic changes that significantly affected palaeoenvironmental conditions in various marine settings (Kouwenhoven and van der Zwaan, 2006; Hüsing *et al.*, 2009). These changes have predominantly been related to tectonic processes in the Gibraltar region, affecting the water exchange with the Atlantic and the palaeo-circulation patterns in the Mediterranean (e.g. Benson *et al.*, 1991; Meijer *et al.*, 2004). Late Tortonian disruptions in the water exchange between the Mediterranean and Atlantic influenced the benthic foraminifera record of the Metochia marls, showing first indications of a restrictive phase between *c.* 8.3 and 8 Ma (Seidenkrantz *et al.*, 2000), roughly coeval with evaporite formation in south-eastern Spain (Krijgsman *et al.*, 2006). It is conceivable that reduced continentality north of Crete, following the disruption of Crete at *c.* 8.2 Ma, altered atmospheric circulation patterns and reduced dust input from the south. These late Tortonian changes in oceanic and atmospheric circulation probably influenced the depositional environments of the Metochia region as well and could explain the inferred change in North African dust proxies. We therefore prefer a hypothesis in which an 8.2 Ma regional tectonic event influenced the climate proxies by altering local or regional depositional environments in the eastern Mediterranean, resulting in reduced African dust deposition in the sink area.

This case study from Gavdos is demonstrative, showing how climate proxies in tectonically active regions, when not combined with independent proxies registering local or regional tectonic changes, can lead to potential misinterpretations. Although we cannot prove the direct cause for the late Tortonian drop of African dust on Gavdos, the tectonic instability and consequent disturbances of local and regional palaeoenvironments in the eastern Mediterranean hamper the straightforward interpretation of proxy changes in terms of African or even global climate.

Conclusions

We studied a multiproxy record from the East Mediterranean Metochia section detecting changes in African climate and Aegean sediment input. Quantification and integration of these proxies show a coeval decrease in Aegean sediment supply and North African dust around 8.2 Ma. The geological record from Crete shows that this event can be correlated in a straightforward manner to the onset of a regional E–W extension related basin foundering. This Aegean tectonic episode coincides with Mediterranean-wide tectonic changes, including the tectonic reorganisation of gateways in the Gibraltar region. Interestingly, these tectonic changes also coincide with an African dust supply in our section, usually associated with a North African climate change towards more humid conditions. Rather than climate change in the source area, the precise synchronicity leads us to associate the change in African dust input to changes in the sink area during the Tortonian restriction phases of the Mediterranean Sea, related to tectonic reorganisations. This study shows the potential of multiproxy analyses to date tectonic events and illustrates that interpretations of climate proxies require a multiproxy approach on well-dated sedimentary records to asses the combined influence of climate and regional tectonics.

Acknowledgements

This study was financed by the DFG International Graduate College EUROPROX. We appreciate discussions with S. Hüsing, and laboratory assistance of T. Frederichs, L. Brück, C. Hilgenfeldt and K. Enneking. L. Jolivet and three anonymous reviewers are thanked for critical reviews.

References

An, Z., Kutzbach, J.E., Prell, J.W. and Porter, S.C., 2001. Evolution of Asian monoons and phased uplift of the Himalaya-Tibetan plateau since Late Miocene times. *Nature*, **411**, 62–66.

Bedzek, J.C., Ehrlich, R. and Full, W., 1984. The fuzzy c-means clustering algorithm. *Comput. Geosci.*, **10**, 191–203.

Benson, R.H., Rakic-El Bied, K. and Bonaduce, G., 1991. An important current reversal (influx) in the Rifian Corridor (Morocco) at the Tortonian-Messinian boundary: the end of the Tethys Ocean. *Paleoceanography*, **6**, 164–192.

Bergametti, G., Gomes, L., Coude-Gaussen, G., Rognon, P., Le Costumer,

M.-N., 1989. African dust observed over Canary Islands: source-regions identification and transport pattern for some summer situations. *J. Geophys. Res.*, **94**, 14855–14864.

Cande, S.C. and Kent, D.V., 1995. Revised calibration of the Geomagnetic Polarity Time Scale for the Late Cretaceous and Cenozoic. *J. Geophys. Res.*, **100**, 6093–6095.

Carminati, E., Wortel, M.J.R., Spakman, W. and Sabadani, R., 1998. The role of slab detachment processes in the opening of the western-central Mediterranean basins: some geological and geophysical evidence. *Earth Planet. Sci. Lett.*, **160**, 651–665.

Fassoulas, C., Kilias, A. and Mountrakis, D., 1994. Postnappe stacking extension and exhumation of high-pressure/low-temperature rocks in the island of Crete, Greece. *Tectonics*, **13**, 127–138.

Fluteau, F., Ramstein, G. and Besse, J., 1999. Simulating the evolution of the Asian and African monsoons during the past 30 Myr using an atmospheric general circulation model. *J. Geophys. Res.*, **104**, 11995–12018.

Fortuin, A.R., 1978. Late Cenozoic history of eastern Crete and implications for the geology and geodynamics of the southern Aegean region. *Geol. Mijnbouw*, **57**, 451–464.

Gladstone, R., Flecker, R., Valdes, P. *et al.*, 2007. The Mediterranean hydrological budget from a Late Miocene global climate simulation. *Palaeogeogr. Palaeoclimatol. Palaeoecol.*, **251**, 254–267.

Griffin, D.L., 2002. Aridity and humidity: two aspects of late Miocene climate of North Africa and the Mediterranean. *Palaeogeogr. Palaeoclimatol. Palaeoecol.*, **182**, 65–91.

Hilgen, F.J., Krijgsman, W., Langereis, C.G. *et al.*, 1995. Extending the astronomical (polarity) time scale into the Miocene. *Earth Planet. Sci. Lett.*, **136**, 495–510.

van Hinsbergen, D.J. and Meulenkamp, J.E., 2006. Neogene supradetachment basin development on Crete (Greece) during exhumation of the South Aegean core complex. *Basin Res.*, **18**, 103–124.

van Hinsbergen, D.J.J., Hafkenscheid, E., Spakman, W. *et al.*, 2005. Nappe stacking resulting from subduction of oceanic and continental lithosphere below Greece. *Geology*, **33**, 325–328.

Hüsing, S.K., Kuiper, K.F., Link, W., Hilgen, F.J. and Krijgsman, W., 2009. The upper Tortonian–lower Messinian at Monte dei Corvi (Northern Apennines; Italy): completing a Mediterranean reference section for the Tortonian Stage. *Earth Planet. Sci. Lett.*, **282**, 140–157.

Jolivet, L., 2001. A comparison of geodetic and finite strain patterns in the Aegean, geodynamic implications. *Earth Planet. Sci. Lett.*, **187**, 95–104.

Jolivet, L., Goffée, B., Monié, P. *et al.*, 1996. Miocene detachment in Crete and exhumation P-T-t paths of high-pressure metamorphic rocks. *Tectonics*, **15**, 1129–1153.

Koepke, J., Seidel, E. and Kreuzer, H., 2002. Ophiolites in the Southern Aegean islands Crete, Karpathos and Rhodes: composition, geochronology and position within the ophiolite belts of the Eastern Mediterranean. *Lithos*, **65**, 183–203.

Köhler, C.M., Heslop, D., Dekkers, M.J. *et al.*, 2008. Tracking provenance changes during the late Miocene in the Eastern Mediterranean Metochia section using geochemical and environmental magnetic proxies. *Geochem. Geophys. Geosyst.*, **9**, Q12018. Doi: 10.1029/2008GC002127.

Kouwenhoven, T.J. and van der Zwaan, G.J., 2006. A reconstruction of late Miocene Mediterranean circulation patterns using benthic foraminifera. *Palaeogeogr. Palaeoclimatol. Palaeoecol.*, **238**, 373–385.

Krijgsman, W., 2002. The Mediterranean: mare nostrum of earth sciences. *Earth Planet. Sci. Lett.*, **205**, 1–12.

Krijgsman, W., Hilgen, F.J., Langereis, C.G. and Zachariasse, W.J., 1994. The age of the Tortonian-Messinian boundary. *Earth Planet. Sci. Lett.*, **121**, 533–547.

Krijgsman, W., Hilgen, F.J., Langereis, C.G. *et al.*, 1995. Late Miocene magnetostratigraphy, biostratigraphy and cyclostratigraphy in the Mediterranean. *Earth Planet. Sci. Lett.*, **136**, 475–494.

Krijgsman, W., Leewis, M.E., Garcés, M. *et al.*, 2006. Tectonic control for evaporite formation in the Eastern Betics (Tortonian; Spain). *Sed. Geol.*, **188–189**, 155–170.

Kroon, D., Steens, T. and Troelstra, S.R., 1991. Onset of monsoonal related upwelling in the western Arabian Sea as revealed by planktonic foraminifers. In: *Proceedings of the Ocean Drilling Program, Scientific Results* (W.L. Prell and N. Niitsuma, eds), pp. 257–263. Ocean Drilling Program, College Station, TX.

Langereis, C.G., 1984. Late Miocene magnetostratigraphy in the Mediterranean. *Geol. Ultraiect.*, **34**, 178.

Larrasoaña, J.C., Roberts, A.P., Rohling, E.J. *et al.*, 2003. Three million years of monsoon variability over the northern Sahara. *Clim. Dyn.*, **21**, 689–698.

Laskar, J., Robutel, P., Joutel, F. *et al.*, 2004. A long-term numerical solution for the insolation quantities of the Earth. *Astron. Astrophys.*, **428**, 261–285.

Le Pichon, X. and Angelier, J., 1981. The Aegean Sea. *Trans. R. Soc. Lond. A*, **300**, 357–372.

Lihoreau, F., Boisserie, J.-R., Viriot, L. *et al.*, 2006. Anthracothere dental anatomy reveals a late Miocene Chado-Libyan bioprovince. *Proc. Natl Acad. Sci. U.S.A.*, **103**, 8763–8767.

Lourens, L.J., Wehausen, R. and Brumsack, H.-J., 2001. Geological constraints on tidal dissipation and dynamical ellipticity of the Earth over the past three million years. *Nature*, **409**, 1029–1033.

Meijer, P.T., Slingerland, R. and Wortel, M.J.R., 2004. Tectonic control on past circulation of the Mediterranean Sea: a model study of the Late Miocene. *Paleoceanography*, **19**, PA1026. Doi: 10.1029/2003PA000956.

deMenocal, P., Bloemendal, J. and King, J.W., 1991. A rock-magnetic record of monsoonal dust deposition to the Arabian Sea: evidence for a shift in the mode of deposition at 2.4 Ma. *Proc. ODP Sci. Res.*, **117**, 389–407.

Meulenkamp, J.E. and Hilgen, F.J., 1986. Event stratigraphy, basin evolution and tectonics of the Hellenic and Calabro-Sicilian arcs. In: *The Origin of Arcs* (F.-C. Wezel, ed.), pp. 327–350. Elsevier, Amsterdam.

Meulenkamp, J.E., Wortel, M.J.R., Van Wamel, W.A. *et al.*, 1988. On the Hellenic subduction zone and the geodynamical evolution of Crete since the late Middle Miocene. *Tectonophysics*, **146**, 203–215.

Rahl, J.M., Anderson, K.M., Brandon, M.T. and Fassoulas, C., 2005. Raman spectroscopic carbonaceous material thermometry of low-grade metamorphic rocks: calibration and application to tectonic exhumation in Crete, Greece. *Earth Planet. Sci. Lett.*, **240**, 339–354.

Rohling, E.J., Cane, T.R., Cooke, S. *et al.*, 2002. African monsoon variability during the previous interglacial maximum. *Earth Planet. Sci. Lett.*, **202**, 61–75.

Ruddiman, W.F., Sarnthein, M., Backman, J., Baldauf, J.G., Curry, W., Dupont, L.M., Janecek, T., Pokras, E.M., Raymo, M.E., Stabell, B., Stein, R. and Tiedemann, R., 1989. Late Miocene to Pleistocene evolution of climate in Africa and the low-latitude Atlantic: overview of Leg 108 results. In: *Proceedings of ODP, Scientific Results* (W.F. Ruddiman, M. Sarnthein *et al.*, eds), pp. 463–484. Ocean Drilling Program, College Station, TX.

Sammon, J.W., 1969. A non-linear mapping for data structure analysis. *IEEE Trans. Comput.*, **C18**, 401–409.

van Santvoort, P.J.M., de Lange, G.J., Langereis, C.G. and Dekkers, M.J., 1997. Geochemical and paleomagnetic evidence for the occurrence of "missing" sapropels in eastern Mediterranean sediments. *Paleoceanography*, **12**, 773–786.

Seidenkrantz, M.-S., Kouwenhoven, T.J., Jorissen, F.J. *et al.*, 2000. Benthic foraminifera as indicators of changing Mediterranean-Atlantic water exchange in the late Miocene. *Mar. Geol.*, **2000**, 387–407.

Sepulchre, P., Ramstein, G., Fluteau, F., Schuster, M., Tiercelin, J.J. and Brunet,

M., 2006. Tectonic uplift and eastern Africa aridification. *Science*, **313**, 1419–1423.

Thomson, S.N., Stöckhert, B. and Brix, M.R., 1998. Thermochronology of the high-pressure metamorphic rocks of Crete, Greece: implications for the speed of tectonic processes. *Geology*, **26**, 259–262.

Wedepohl, K.H. (ed.), 1969. Composition and abundances of common igneous rocks. In: *Handbook of Geochemistry*, 444 pp. Springer, Berlin.

Wehausen, R. and Brumsack, H.-J., 1998. The formation of Pliocene Mediterranean sapropels: constraints from high-resolution major and minor element studies. In: *Proceedings of the Ocean Drilling Program, Scientific Results* (A.H.F. Robertson, K.-C. Emeis and A. Camerlenghi, eds), pp. 207–217. Ocean Drilling Program, College Station, TX.

Wehausen, R. and Brumsack, H.-J., 2000. Chemical cycles in Pliocene sapropel-bearing and sapropel barren eastern Mediterranean sediments. *Palaeogeogr. Palaeoclimatol. Palaeoecol.*, **158**, 325–352.

Wortel, M.J.R. and Spakman, W., 2000. Subduction and slab detachment in the Mediterranean-Carpathian region. *Science*, **290**, 1910–1917.

Received 3 September 2008; revised version accepted 11 October 2009

Appendix A

Table of the analytical data used in this study: sedimentation rate, geochemical and environmental magnetic proxies of the samples of the Metochia section

Age (Ma)	Sedimentation Rate (cm ka^{-1})	Ca (mg kg^{-1})	$CaCO_3$ (%)	Al (mg kg^{-1})	Al-MAR (kg m^{-2} ka^{-1})	Ni (mg kg^{-1})	Ni-MAR (kg m^{-2} ka^{-1})	Cr (mg kg^{-1})	Cr-MAR (kg m^{-2} ka^{-1})	Mn/Al	Ti/Al	$HIRM_{cfb}$ (mA m^{-1})	ARM_{cfb} (mA m^{-1})
9.426	6.6	161300	39.5	51050	22221	95.5	41.57	159	69.21	0.0051	0.0512	397.69	29.30
9.422	6.6	156000	38.2	47040	20475	121.5	52.89	179	77.91	0.0081	0.0725	432.25	28.86
9.418	5.5	127000	31.1	56090	16967	109.8	33.21	168	50.82	0.0056	0.0605	107.37	15.07
9.411	5.5	141100	34.5	68220	20637	133.2	40.29	152	45.98	0.0050	0.0439	373.64	22.13
9.404	5.5	201700	49.4	49200	14883	75.1	22.72	153	46.28	0.0071	0.0495	375.18	28.35
9.401	5.5	144600	35.4	58280	17630	153.2	46.34	199	60.20	0.0123	0.0583	258.71	30.25
9.383	4.01	147000	36.0	60060	9648	128.3	20.61	219	35.18	0.0056	0.0549	385.49	25.93
9.380	4.01	170900	41.8	52500	8434	117.9	18.94	198	31.81	0.0113	0.0634	414.18	28.10
9.376	4.01	163200	39.9	56510	9078	105.5	16.95	222	35.66	0.0082	0.0543	469.85	35.92
9.374	4.01	154500	37.8	59590	9573	115.1	18.49		27.79	0.0064	0.0542	381.86	34.30
9.353	3.53	178800	43.8	45540	5676	121.7	15.17		25.18	0.0064	0.0656	454.16	38.84
9.344	3.53	227900	55.8	79390	9895	197.0	173	245	30.54	0.0060	0.0636	612.13	47.13
9.338	3.53	245400	60.1	63510	7916	148.4	202	219	27.30	0.0071	0.0700	658.87	63.46
9.330	3.53	167500	41.0	49200	6130	111.2	13.86	134	16.70	0.0076	0.0584	548.73	39.14
9.309	3.51	165200	40.4	47870	5909	115.3	14.23	208	25.68	0.0095	0.0688	402.70	41.20
9.301	3.51	175300	42.9	49870	6156	126.3	15.59	210	25.92	0.0078	0.0562	243.75	31.45
9.294	3.51	183400	44.9	50860	6279	128.9	15.91	126	15.55	0.0115	0.0566	145.35	15.56
9.275	3.87	180500	44.2	44350	6637	129.3	19.35	218	32.62	0.0102	0.0687	90.78	8.80
9.271	3.82	181000	44.3	47130	6867	111.2	16.20	166	24.19	0.0076	0.0598	13.81	8.07
9.260	3.63	152400	37.3	58470	7706	160.9	21.21	191	25.17	0.0083	0.0648	11.69	7.09
9.257	3.63	145900	35.7	43420	5723	112.2	14.79	236	31.10	0.0077	0.0720	254.13	8.80
9.250	3.63	157500	38.5	51010	6723	130.2	17.16	184	24.25	0.0084	0.0599	39.47	8.60
9.234	3.6	165800	40.6	46740	6058	119.1	15.44	216	27.99	0.0086	0.0654	29.00	8.73
9.228	3.34	172700	42.3	50820	5661	133.5	14.87	234	26.07	0.0092	0.0635	11.71	5.45
9.219	3.15	168700	41.3	53450	5311	122.8	12.20	126	12.52	0.0060	0.0509	17.14	7.07
9.212	3.15	182300	44.6	47500	4720	115.9	11.52	202	20.07	0.0086	0.0592	45.06	9.74
9.184	3.46	157900	38.6	58420	6980	100.2	11.97	160	19.12	0.0058	0.0587	38.84	7.11
9.165	3.86	183100	44.8	50010	7440	134.1	19.95	253	37.64	0.0055	0.0559	72.47	8.21
9.160	3.86	151100	37.0	54120	8052	100.9	15.01	154	22.91	0.0056	0.0650	111.95	7.94
9.142	3.52	162400	39.7	52490	6510	118.6	14.71	167	20.71	0.0072	0.0634	32.47	8.08
9.140	3.52	161700	39.6	56630	7024	100.6	12.48	206	25.55	0.0053	0.0591	14.64	8.01
9.136	3.52	179700	44.0	47190	5853	101.6	12.60	152	18.85	0.0082	0.0630	15.99	9.34
9.133	3.52	189400	46.4	46920	5819	119.2	14.78	216	26.79	0.0092	0.0639	104.45	9.94
9.118	3.7	196100	48.0	40920	5602	126.8	17.36	188	25.74	0.0089	0.0709	20.19	7.19
9.113	3.7	190200	46.5	50180	6870	96.2	13.17	209	28.61	0.0068	0.0529	15.29	6.27
9.110	3.7	178700	43.7	52850	7235	131.7	18.03	176	24.09	0.0073	0.0611	44.60	9.69
9.096	3.72	153700	37.6	61370	8481	104.7	14.47	162	22.39	0.0053	0.0554	23.76	8.55
9.093	3.72	156600	38.3	60990	8428	101.5	14.03	152	21.00	0.0052	0.0578	43.48	8.12
9.090	3.72	152800	37.4	62850	8685	137.6	19.01	207	28.61	0.0094	0.0559	20.17	8.70
9.087	3.72	160100	39.2	60640	8380	122.1	16.87	163	22.52	0.0060	0.0555	97.68	9.47
9.070	3.14	152300	37.3	60810	5982	126.2	12.41	205	20.17	0.0049	0.0556	35.26	7.91

Appendix A
Continued

Age (Ma)	Sedimentation Rate (cm ka^{-1})	Ca (mg kg^{-1})	$CaCO_3$ (%)	Al (mg kg^{-1})	Al-MAR (kg m^{-2} ka^{-1})	Ni (mg kg^{-1})	Ni-MAR (kg m^{-2} ka^{-1})	Cr (mg kg^{-1})	Cr-MAR (kg m^{-2} ka^{-1})	Mn/Al	Ti/Al	$HIRM_{cfb}$ (mA m^{-1})	ARM_{cfb} (mA m^{-1})
9.067	3.14	146800	35.9	62700	6168	125.0	12.30	179	17.61	0.0055	0.0574	23.96	8.93
9.064	3.14	156200	38.2	54910	5401	123.1	12.11	217	21.35	0.0064	0.0636	23.76	9.22
9.048	3.57	146600	35.9	61730	7859	122.8	15.63	191	24.32	0.0058	0.0606	17.09	7.69
9.045	3.57	146700	35.9	60580	7713	120.1	15.29	184	23.43	0.0062	0.0555	36.82	6.97
9.042	3.57	164200	40.2	52770	6719	135.3	17.23	184	23.43	0.0065	0.0609	142.85	9.30
9.028	2.93	162000	39.6	79030	6778	125.6	10.77	225	19.30	0.0047	0.0401	52.92	9.99
9.019	2.93	148800	36.4	68540	5878	119.2	10.22	169	14.49	0.0062	0.0315	203.18	8.12
9.009	3.03	129200	31.6	73880	6803	204.8	18.86	207	19.06	0.0064	0.0397	65.77	8.43
9.004	3.03	173300	42.4	60610	5581	290.2	26.72	243	22.38	0.0367	0.0470	252.90	9.72
9.000	3.03	160900	39.4	65260	6009	125.6	11.57	163	15.01	0.0057	0.0418	275.80	8.72
8.996	3.03	170400	41.7	59780	5505	128.9	11.87	189	17.40	0.0069	0.0484	153.98	9.05
8.991	3.03	172400	42.2	53580	4934	161.4	14.86	118	10.87	0.0114	0.0539	350.05	9.61
8.979	3	155400	38.0	62020	5582	157.6	14.18	181	16.29	0.0064	0.0576	29.03	11.13
8.971	3	168300	41.2	54840	4936	154.7	13.92	204	18.36	0.0066	0.0496	168.49	7.70
8.953	2.95	171700	42.0	58180	5071	114.3	9.96	138	12.03	0.0059	0.0531	35.99	7.78
8.949	2.95	210400	51.5	44970	3920	131.3	11.44	199	17.35	0.0085	0.0598	84.86	8.46
8.937	2.98	155400	38.0	59210	5245	178.9	15.85	275	24.36	0.0074	0.0487	16.64	8.81
8.932	2.98	163300	40.0	59960	5311	153.4	13.59	173	15.32	0.0097	0.0525	23.77	7.88
8.927	2.98	206100	50.4	44010	3898	109.6	9.71	157	13.91	0.0090	0.0617	53.38	9.39
8.916	2.41	165000	40.4	57420	3325	211.3	12.23	213	12.33	0.0058	0.0455	45.73	8.74
8.912	2.41	201100	49.2	48250	2794	149.6	8.66	214	12.39	0.0081	0.0556	100.61	10.77
8.910	2.41	213800	52.3	45760	2650	153.4	8.88	189	10.94	0.0092	0.0539	36.11	8.92
8.902	2.89	194500	47.6	53620	4493	140.6	11.78	171	14.33	0.0065	0.0469	48.82	9.67
8.899	2.89	200100	49.0	48100	4031	108.5	9.09	153	12.82	0.0086	0.0586	171.63	10.09
8.896	2.89	216000	52.9	45080	3777	99.0	8.30	205	17.18	0.0085	0.0650	103.52	11.75
8.892	2.89	199300	48.8	49800	4173	132.6	11.11	145	12.15	0.0084	0.0562	71.93	9.38
8.883	3.8	163100	39.9	50820	7338	170.9	24.68	159	22.96	0.0078	0.0547	16.82	6.87
8.879	3.8	167900	41.1	59030	8524	109.6	15.83	193	27.87	0.0074	0.0559	252.87	8.37
8.876	3.8	163100	39.9	56770	8198	105.7	15.26	172	24.84	0.0064	0.0588	150.95	8.43
8.873	3.8	188000	46.0	53290	7695	126.6	18.28	190	27.44	0.0079	0.0547	29.50	10.93
8.860	3.03	197200	48.3	46810	4287	131.2	12.02	148	13.55	0.0083	0.0594	93.77	11.89
8.857	3.03	214100	52.4	45820	4196	98.0	8.98	157	14.38	0.0086	0.0581	354.88	11.93
8.854	3.03	191800	46.9	49640	4546	158.7	14.53	218	19.97	0.0081	0.0589	171.26	8.94
8.844	2.65	207200	50.7	45070	3158	110.0	7.71	146	10.23	0.0076	0.0605	191.13	11.72
8.834	2.65	209800	51.3	46090	3229	128.9	9.03	119	8.34	0.0092	0.0578	112.61	10.17
8.817	3.19	189700	46.4	50050	5095	93.0	9.47	158	16.08	0.0065	0.0610	146.28	8.91
8.810	3.19	194600	47.6	46670	4751	101.5	10.33	124	12.62	0.0080	0.0708	60.37	8.67
8.805	3.19	201200	49.2	47970	4883	115.2	11.73	190	19.34	0.0086	0.0630	88.69	9.76
8.786	3.52	176100	43.1	56450	7014	106.0	13.17	197	24.48	0.0056	0.0545	49.41	9.21
8.783	3.53	186200	45.6	51350	6381	93.7	11.64	125	15.53	0.0062	0.0599	331.34	9.64
8.780	3.52	188500	46.1	47780	5937	106.3	13.21	184	22.86	0.0077	0.0656	57.06	10.88
8.763	3.13	171100	41.9	53330	5208	226.4	22.11	176	17.19	0.0246	0.0600	32.45	10.47

Appendix A
Continued

Age (Ma)	Sedimentation Rate (cm ka^{-1})	Ca (mg kg^{-1})	$CaCO_3$ (%)	Al (mg kg^{-1})	Al-MAR (kg m^{-2} ka^{-1})	Ni (mg kg^{-1})	Ni-MAR (kg m^{-2} ka^{-1})	Cr (mg kg^{-1})	Cr-MAR (kg m^{-2} ka^{-1})	Mn/Al	Ti/Al	$HIRM_{cfb}$ (mA m^{-1})	ARM_{cfb} (mA m^{-1})
8.760	3.12	293700	71.9	76780	7498	92.4	9.02	126	12.30	0.0055	0.0613	153.88	17.65
8.756	3.05	195400	47.8	48210	4484	112.9	10.50	144	13.39	0.0092	0.0564	136.24	11.50
8.736	2.3	232700	56.9	40130	2114	98.3	5.18	206	10.85	0.0102	0.0570	20.45	15.21
8.730	2.29	223700	54.7	44590	2349	157.5	8.30	200	10.53	0.0221	0.0503	17.44	13.53
8.724	2.3	235400	57.6	39870	2100	78.8	4.15	148	7.80	0.0135	0.0573	24.75	16.98
8.717	2.29	216000	52.9	48340	2546	90.7	4.78	116	6.11	0.0140	0.0518	18.25	12.24
8.713	2.3	216500	53.0	46800	2465	81.5	4.29	170	8.95	0.0094	0.0548	29.03	12.69
8.694	3.55	195300	47.8	50390	6334	100.7	12.66	148	18.60	0.0069	0.0606	44.05	11.64
8.689	3.55	189200	46.3	52940	6655	87.1	10.95	158	19.86	0.0058	0.0594	131.37	10.40
8.687	3.55	210700	51.6	48970	6156	140.9	17.71	138	17.35	0.0186	0.0556	22.21	11.91
8.673	3.9	196700	48.1	47810	7290	102.7	15.66	188	28.66	0.0081	0.0600	71.17	12.22
8.670	3.9	199800	48.9	50120	7642	81.3	12.40	124	18.91	0.0065	0.0652	43.21	10.62
8.666	3.9	184600	45.2	51310	7823	104.7	15.96	211	32.17	0.0056	0.0587	161.14	11.00
8.649	3.5	183400	44.9	53610	6567	93.7	11.48	166	20.34	0.0070	0.0579	14.50	7.71
8.645	3.5	202500	49.6	48990	6001	75.2	9.21	157	19.23	0.0078	0.0606	30.23	11.38
8.641	3.5	205300	50.2	43470	5325	110.4	13.52	170	20.83	0.0132	0.0610	83.85	19.36
8.632	2.64	224300	54.9	40610	2839	102.8	7.19	152	10.63	0.0107	0.0584	436.05	69.20
8.625	2.64	246600	60.4	36290	2537	93.4	6.53	116	8.11	0.0136	0.0589	472.02	48.16
8.620	2.64	245200	60.0	37490	2621	75.8	5.30	142	9.93	0.0132	0.0638	463.40	67.47
8.607	2.64	220000	53.8	42700	2986	84.8	5.93	146	10.21	0.0091	0.0606	513.76	59.36
8.596	2.64	239900	58.7	38510	2693	69.0	4.82	131	9.16	0.0110	0.0607	632.53	74.36
8.577	3.36	238900	58.5	37810	4281	85.5	9.68	160	18.11	0.0112	0.0677	389.75	42.20
8.570	3.38	190800	46.7	48150	5504	118.3	13.52	156	17.83	0.0067	0.0482	211.41	40.20
8.563	3.38	240200	58.8	33830	3867	48.1	5.50	99	11.32	0.0133	0.0642	330.28	49.15
8.560	2.22	239700	58.7	36220	1783	78.0	3.84	155	7.63	0.0154	0.0626	768.28	39.06
8.552	2.22	221100	54.1	44140	2173	92.1	4.53	153	7.53	0.0130	0.0592	970.12	59.59
8.517	2.22	230200	56.3	38110	1876	107.8	5.31	151	7.43	0.0158	0.0652	906.44	93.62
8.494	2.22	216000	52.9	45440	2237	80.6	3.97	119	5.86	0.0122	0.0563	1042.78	98.92
8.487	2.22	210900	51.6	44090	2170	130.6	6.43	160	7.88	0.0143	0.0694	820.36	86.46
8.480	2.22	211500	51.8	44940	2212	70.3	3.46	146	7.19	0.0122	0.0542	1113.74	159.02
8.474	2.22	222800	54.5	43780	2155	86.3	4.25	177	8.71	0.0119	0.0610	1313.02	74.16
8.469	2.22	259200	63.4	27310	1344	83.2	4.10	102	5.02	0.0219	0.0772	808.18	148.45
8.449	2.22	196200	48.0	45340	2232	101.2	4.98	85	4.18	0.0088	0.0549	39.20	63.83
8.441	2.22	204000	49.9	41080	2022	68.8	3.39	107	5.27	0.0093	0.0651	197.79	8.09
8.435	2.22	238800	58.4	34190	1683	71.1	3.50	156	7.68	0.0170	0.0630	510.82	89.98
8.423	2.22	245100	60.0	33350	1641	67.8	3.34	119	5.86	0.0161	0.0586	557.39	42.30
8.415	2.22	241700	59.2	36980	1820	74.6	3.67	151	7.43	0.0138	0.0535	23.48	39.84
8.406	2.63	192200	47.0	46400	3214	72.1	4.99	148	10.25	0.0080	0.0600	12.86	11.62
8.397	3.88	213600	52.3	46880	7061	64.3	9.68	128	19.28	0.0099	0.0649	13.67	7.56
8.392	3.88	235700	57.7	41820	6299	86.1	12.97	113	17.02	0.0155	0.0602	25.55	11.70
8.389	3.88	184000	45.0	42850	6454	44.4	6.69	90	13.56	0.0142	0.0594	13.22	6.16
8.387	3.88	194300	47.6	49020	7383	96.1	14.47	162	24.40	0.0077	0.0601	606.66	37.50

Appendix A
Continued

Age (Ma)	Sedimentation Rate (cm ka^{-1})	Ca (mg kg^{-1})	$CaCO_3$ (%)	Al (mg kg^{-1})	Al-MAR (kg m^{-2} ka^{-1})	Ni (mg kg^{-1})	Ni-MAR (kg m^{-2} ka^{-1})	Cr (mg kg^{-1})	Cr-MAR (kg m^{-2} ka^{-1})	Mn/Al	Ti/Al	$HIRM_{cfb}$ (mA m^{-1})	ARM_{cfb} (mA m^{-1})
8.362	3.54	218500	53.5	42580	5341	45.5	5.71	171	21.45	0.0166	0.0578	430.22	9.33
8.336	2.66	187100	45.8	46240	3280	83.1	5.89	122	8.65	0.0085	0.0692	253.25	25.56
8.329	2.66	182000	44.5	44140	3131	90.2	6.40	130	9.22	0.0103	0.0630	173.40	26.18
8.317	2.66	238300	58.3	31170	2211	79.9	5.67	122	8.65	0.0152	0.0667	300.74	41.90
8.311	2.66	220500	54.0	34650	2458	68.3	4.84	137	9.72	0.0148	0.0635	151.31	30.15
8.286	3.98	199100	48.7	44350	7012	77.9	12.32	153	24.19	0.0106	0.0586	280.67	6.27
8.273	3.86	193200	47.3	43500	6472	110.3	16.41	125	18.60	0.0085	0.0633	338.99	6.99
8.267	3.86	194600	47.6	44290	6589	90.8	13.51	124	18.45	0.0109	0.0638	331.90	7.21
8.247	4.74	191700	46.9	51760	11625	82.2	18.46	123	27.63	0.0078	0.0605	149.81	13.76
8.243	4.74	209400	51.2	47220	10605	86.4	19.40	153	34.36	0.0080	0.0595	297.41	29.11
8.216	3.39	229700	56.2	38980	4480	74.4	8.55	105	12.07	0.0114	0.0585	652.60	41.33
8.210	3.39	180600	44.2	50280	5778	70.1	8.06	108	12.41	0.0086	0.0553	653.71	31.52
8.193	3.39	220800	54.0	43460	4994	93.5	10.75	156	17.93	0.0114	0.0540	516.42	40.74
8.180	4.82	169500	41.5	46680	10826	103.0	23.89	101	23.42	0.0171	0.0587	471.13	28.25
8.177	4.82	182700	44.7	49040	11373	57.4	13.31	91	21.10	0.0062	0.0643	839.88	28.25
8.173	4.82	226400	55.4	40130	9307	53.5	12.41	87	20.18	0.0132	0.0615	948.71	31.12
8.158	3.83	216600	53.0	46940	6898	94.3	13.86	110	16.16	0.0135	0.0417	155.72	28.45
8.155	3.83	170400	41.7	45810	6732	86.8	12.75	145	21.31	0.0103	0.0599	614.49	30.21
8.151	3.83	203500	49.8	43200	6348	74.8	10.99	130	19.10	0.0100	0.0622	143.79	27.87
8.129	2.69	201800	49.4	51180	3704	55.2	4.00	138	9.99	0.0099	0.0540	27.22	12.52
8.125	2.69	202400	49.5	49720	3599	60.4	4.37	151	10.93	0.0102	0.0507	16.23	11.67
8.121	2.69	201200	49.2	46940	3398	79.7	5.77	96	6.95	0.0099	0.0563	12.16	12.59
8.116	2.69	228100	55.8	41660	3015	72.7	5.26	141	10.21	0.0112	0.0502	22.08	15.93
8.108	2.69	221200	54.1	41970	3038	84.8	6.14	137	9.92	0.0133	0.0539	13.96	13.81
8.097	2.69	211000	51.6	44720	3237	72.0	5.21	175	12.67	0.0113	0.0584	56.72	14.19
8.091	2.69	251500	61.6	36630	2651	74.1	5.36	105	7.60	0.0164	0.0519	19.73	15.45
8.085	2.69	234500	57.4	36130	2615	73.7	5.33	112	8.11	0.0131	0.0650	21.18	11.55
8.061	2.69	200900	49.2	44730	3238	91.9	6.65	187	13.54	0.0116	0.0542	12.70	16.80
8.048	2.69	230900	56.5	39990	2895	104.2	7.54	138	9.99	0.0165	0.0512	15.52	14.97
8.042	2.69	235900	57.7	40480	2930	69.6	5.04	126	9.12	0.0130	0.0563	14.61	11.60
8.038	2.69	217500	53.2	47150	3413	91.9	6.65	169	12.23	0.0109	0.0531	13.77	11.03
8.035	2.69	213800	52.3	44500	3221	65.2	4.72	122	8.83	0.0110	0.0550	21.29	9.79
8.004	3.21	197400	48.3	48910	5048	62.1	6.41	124	12.80	0.0088	0.0561	17.74	8.22
8.000	3.21	228600	55.9	43640	4504	44.1	4.55	76	7.84	0.0126	0.0560	14.21	8.48
7.997	3.21	233700	57.2	40360	4165	70.4	7.27	128	13.21	0.0132	0.0524	13.83	7.54
7.991	2.68	190500	46.6	46230	3325	107.2	7.71	153	11.00	0.0105	0.0438	9.35	7.11
7.989	2.68	202500	49.6	47960	3449	93.8	6.75	162	11.65	0.0099	0.0553	19.40	7.90
7.957	2.14	205700	50.3	43980	2014	76.3	3.49	120	5.50	0.0087	0.0583	18.89	6.03
7.952	2.14	227800	55.8	38880	1781	74.4	3.41	153	7.01	0.0118	0.0587	28.35	8.29
7.934	2.14	161600	39.5	41910	1919	284.2	13.02	173	7.92	0.0454	0.0602	334.18	7.43
7.915	2.5	228700	56.0	40970	2561	76.2	4.76	123	7.69	0.0134	0.0593	43.60	8.65
7.912	2.5	208200	51.0	49040	3065	57.1	3.57	129	8.06	0.0106	0.0556	41.92	7.62
7.910	2.5	204900	50.1	48510	3032	65.3	4.08	99	6.19	0.0102	0.0522	56.81	7.33

Appendix A
Continued

Age (Ma)	Sedimentation Rate (cm ka^{-1})	Ca (mg kg^{-1})	$CaCO_3$ (%)	Al (mg kg^{-1})	Al-MAR (kg m^{-2} ka^{-1})	Ni (mg kg^{-1})	Ni-MAR (kg m^{-2} ka^{-1})	Cr (mg kg^{-1})	Cr-MAR (kg m^{-2} ka^{-1})	Mn/Al	Ti/Al	$HIRM_{cfb}$ (mA m^{-1})	ARM_{cfb} (mA m^{-1})
7.896	2.52	199400	48.8	49980	3184	147.0	9.36	156	9.94	0.0136	0.0446	19.18	5.38
7.891	2.52	209100	51.2	48500	3089	58.2	3.71	133	8.47	0.0108	0.0548	31.94	4.85
7.871	2.98	197500	48.3	42950	3810	107.8	9.56	133	11.80	0.0166	0.0553	97.92	7.36
7.868	2.98	231200	56.6	38410	3407	63.8	5.66	110	9.76	0.0178	0.0569	57.99	4.82
7.864	2.98	226800	55.5	42340	3756	77.7	6.89	111	9.85	0.0120	0.0532	20.65	4.77
7.783	2.14	222400	54.4	46220	2110	107.1	4.89	135	6.16	0.0112	0.0416	18.87	7.56
7.755	1.9	233700	57.2	39360	1428	74.7	2.71	116	4.21	0.0144	0.0622	16.98	13.48
7.749	1.9	223100	54.6	46640	1692	82.6	3.00	169	6.13	0.0082	0.0452	22.60	11.88
7.743	1.9	242500	59.3	40050	1453	89.9	3.26	144	5.22	0.0139	0.0500	22.62	16.95
7.726	1.9	230700	56.5	44870	1628	83.7	3.04	161	5.84	0.0122	0.0502	13.69	13.60
7.713	1.9	247300	60.5	41650	1511	76.2	2.76	144	5.22	0.0150	0.0465	12.53	15.71
7.696	1.9	254100	62.2	36540	1325	78.3	2.84	156	5.66	0.0192	0.0475	12.46	15.75
7.685	1.9	237300	58.1	43410	1575	71.1	2.58	143	5.19	0.0101	0.0442	14.61	15.75
7.657	1.9	275700	67.5	28840	1046	82.0	2.97	101	3.66	0.0196	0.0583	16.39	27.19
7.644	1.9	249100	61.0	33910	1230	80.3	2.91	105	3.81	0.0147	0.0506	24.70	19.55
7.632	1.9	229100	56.1	38930	1412	57.2	2.07	90	3.26	0.0103	0.0593	15.00	13.93
7.624	1.9	227300	55.6	41840	1518	66.2	2.40	123	4.46	0.0104	0.0592	19.06	10.82
7.616	1.9	254500	62.3	35590	1291	77.5	2.81	147	5.33	0.0136	0.0489	19.88	15.51
7.598	1.9	276800	67.7	30650	1112	58.2	2.11	89	3.23	0.0140	0.0552	7.40	10.50
7.564	2.36	271500	66.4	26070	1456	50.9	2.84	148	8.27	0.0261	0.0582	114.45	15.61
7.507	2.27	231000	56.5	36460	1882	60.0	3.10	135	6.97	0.0138	0.0620	15.26	8.20
7.465	2.3	221300	54.2	44440	2346	51.9	2.74	132	6.97	0.0086	0.0575	10.32	7.30
7.433	2.3	209400	51.2	41650	2198	71.6	3.78	140	7.39	0.0084	0.0496	18.97	7.37
7.419	2.3	229800	56.2	42020	2218	56.0	2.96	167	8.81	0.0079	0.0571	10.56	10.42
7.394	2.3	253800	62.1	35480	1873	51.4	2.71	141	7.44	0.0095	0.0570	16.14	13.55
7.384	2.3	282800	69.2	28500	1504	52.2	2.76	92	4.86	0.0227	0.0506	17.25	13.19
7.366	2.3	255100	62.4	37170	1962	78.7	4.15	80	4.22	0.0139	0.0531	11.90	12.66
7.356	1.92	248700	60.9	35460	1314	76.2	2.82	103	3.82	0.0186	0.0252	9.25	13.04
7.353	1.93	256500	62.8	33850	1254	66.1	2.45	103	3.82	0.0122	0.0532	17.40	15.21
7.346	1.92	212800	52.1	46420	1720	67.1	2.49	146	5.41	0.0081	0.0560	13.90	10.84
7.342	1.92	265100	64.9	29750	1102	59.7	2.21	107	3.97	0.0159	0.0706	17.91	14.42
7.334	1.93	273000	66.8	27990	1037	81.6	3.02	154	5.71	0.0250	0.0596	16.09	14.89
7.314	1.93	262400	64.2	33300	1234	61.4	2.28	74	2.74	0.0168	0.0453	15.98	15.74
7.294	1.93	251600	61.6	37900	1404	56.6	2.10	106	3.93	0.0118	0.0501	12.20	11.13
7.287	1.93	269700	66.0	30410	1127	60.2	2.23	175	6.48	0.0160	0.0574	11.88	10.02
7.280	1.92	253600	62.1	29590	1096	59.8	2.22	158	5.85	0.0204	0.0582	8.33	12.64
7.262	1.93	238200	58.3	38430	1424	51.3	1.90	128	4.74	0.0143	0.0552	37.24	8.57
7.257	1.92	242500	59.3	34260	1268	68.3	2.53	139	5.15	0.0174	0.0581	11.91	9.37
7.223	1.9	229000	56.0	33690	1214	53.7	1.94	120	4.33	0.0180	0.0622	13.78	10.11
7.207	1.9	249200	61.0	34480	1243	63.4	2.29	120	4.33	0.0200	0.0539	11.79	9.77